JVI Journals.ASM.org

Varicella-Zoster Virus Inhibition of the NF-κB Pathway during Infection of Human Dendritic Cells: Role for Open Reading Frame 61 as a Modulator of NF-κB Activity

Elizabeth Sloan,[a,b] Rodney Henriquez,[a,b] Paul R. Kinchington,[c] Barry Slobedman,[a,b] and Allison Abendroth[a,b]

Centre for Virus Research, Westmead Millennium Institute,[a] and Department of Infectious Diseases and Immunology, University of Sydney,[b] Sydney, Australia, and Departments of Ophthalmology and Molecular Microbiology and Genetics, University of Pittsburgh, Pittsburgh, Pennsylvania, USA[c]

Dendritic cells (DC) are antigen-presenting cells essential for initiating primary immune responses and therefore an ideal target for viral immune evasion. Varicella-zoster virus (VZV) can productively infect immature human DCs and impair their function as immune effectors by inhibiting their maturation, as evidenced by the expression modulation of functionally important cell surface immune molecules CD80, CD86, CD83, and major histocompatibility complex I. The NF-κB pathway largely regulates the expression of these immune molecules, and therefore we sought to determine whether VZV infection of DCs modulates the NF-κB pathway. Nuclear localization of NF-κB p50 and p65 indicates pathway activation; however, immunofluorescence studies revealed cytoplasmic retention of these NF-κB subunits in VZV-infected DCs. Western blotting revealed phosphorylation of the inhibitor of κBα (IκBα) in VZV-infected DCs, indicating that the pathway is active at this point. We conclude that VZV infection of DC inhibits the NF-κB pathway following protein phosphorylation but before the translocation of NF-κB subunits into the nucleus. An NF-κB reporter assay identified VZV open reading frame 61 (ORF61) as an inhibitor of tumor necrosis factor alpha-induced NF-κB reporter activity. Mutational analysis of ORF61 identified the E3 ubiquitin ligase domain as a region required for NF-κB pathway inhibition. In summary, we provide evidence that VZV inhibits the NF-κB signaling pathway in human DCs and that the E3 ubiquitin ligase domain of ORF61 is required to modulate this pathway. Thus, this work identifies a mechanism by which VZV modulates host immune function.

Varicella-zoster virus (VZV) is an alphaherpesvirus causing chickenpox (varicella) during primary infection and shingles (herpes zoster) following reactivation from a latent infection. Following initial exposure to the virus, there is a 10- to 21-day incubation period before the appearance of the varicella rash. During this time it has been proposed that VZV actively evades immune recognition in this period, since the development of adaptive immunity is delayed (reviewed in reference 1). We have postulated that VZV infection of dendritic cells (DCs) and/or modulation of the immune function of these potent antigen-presenting cells would provide a strategy that would enhance the capacity of the virus to be transported from the site of inoculation to the draining lymph nodes to infect T cells while also evading immune detection.

We have previously shown that VZV can productively infect human DCs *in vitro* and *in vivo* (2, 16, 22). These studies included demonstration that productively infected immature monocyte-derived DCs (MDDCs) are unable to upregulate the functionally important immune molecules CD80, CD83, CD86, major histocompatibility complex I, and CCR7, which are required for DC maturation and induction of an effective antiviral immune response (2). The expression of the immune molecules inhibited by VZV are largely regulated by the nuclear factor κB (NF-κB) signal transduction pathway (4, 6, 12–14). The NF-κB signal transduction pathway is an important regulator of innate immunity and inflammation that is triggered by a wide variety of stimuli, including virus infection, tumor necrosis factor alpha (TNF-α), and other cytokines and pathogens (26, 29). Activation of the NF-κB pathway via pattern recognition receptors results in the phosphorylation of inhibitor of κB kinase complex (IKK), which in turn phosphorylates IκB, targeting it for ubiquitination and degradation, allowing NF-κB proteins (p50 and p65) to translocate into the nucleus and bind to promoters containing NF-κB response elements, initiating transcription of target genes (reviewed in references 26 and 29).

Herpesviruses encode multiple proteins that function in immune evasion, and several herpesvirus proteins target and disrupt the NF-κB pathway. Viral genes encoded by Epstein-Barr virus (19, 27, 28), cytomegalovirus (23, 34), and herpes simplex virus 1 (HSV-1) (3, 9, 24) have been identified to regulate the NF-κB pathway in a cell type-dependent manner. Jones and Arvin (17) reported that VZV inhibits the NF-κB pathway in human fibroblasts *in vitro* and *in vivo* following the phosphorylation and ubiquitination of IκBα but prior to the translocation of NF-κB proteins into the nucleus.

In the present study, we sought to extend these studies and examine the effect of VZV on the NF-κB pathway within VZV-infected human MDDCs. Using flow cytometry, immunofluorescent staining, and Western blotting, we establish the point where VZV impacts the NF-κB pathway in VZV antigen-positive DCs. In addition, using a transient-transfection approach and flow cytometry, we identified the E3 ubiquitin ligase domain of VZV ORF61 as responsible for the inhibition of TNF-α-induced NF-κB re-

Received 1 October 2011 **Accepted** 3 November 2011
Published ahead of print 16 November 2011
Address correspondence to Allison Abendroth, allison.abendroth@sydney.edu.au.
B. Slobedman and A. Abendroth contributed equally to this article.

doi:10.1128/JVI.06400-11

porter activity. In summary, we provide evidence here that VZV inhibits the NF-κB signaling pathway in human DCs and define a role for ORF61 as a modulator of this pathway.

MATERIALS AND METHODS

Viruses and cell culture. Peripheral blood mononuclear cells were isolated from healthy adult donors by Ficoll-Hypaque density gradient (Amersham Pharmacia Biotech, Sweden) in accordance with University of Sydney Human Ethics Approval. Monocytes were isolated by CD14 magnetic bead separation (MACS Miltenyi Biotec, Germany) and resuspended at 5×10^5 cells/ml in RPMI (Gibco, Gaithersburg, MD) containing 10% heat-inactivated fetal bovine serum (FBS; CSL, Australia) supplemented with interleukin-4 (IL-4; Schering-Plough, Germany) at 500 U/ml and granulocyte-macrophage-colony-stimulating factor (GMCSF; Schering-Plough, Germany) at 400 U/ml. Cells were cultured for 6 days. Typically, >90% of the MDDCs were shown by flow cytometry analysis to be $CD1a^+/CD14^-$ and have an immature dendritic cell phenotype as we have previously described (2).

Human foreskin fibroblasts (HFFs; American Type Culture Collection) and human embryonic kidney cells (293FT; Invitrogen) were cultured in Dulbecco modified Eagle medium (DMEM; Gibco, Gaithersburg, MD) containing 10% heat-inactivated FBS and 1% PenStrep. Recombinant OKA (rOKA) VZV, kindly provided by A. M. Arvin, Stanford University, was propagated in HFFs and used for cell-associated infections when 60 to 80% of cells were infected. HSV-1 strain (CW) was kindly provided by A. L. Cunningham, Westmead Millennium Institute (20).

TNF-α-treated HFFs, MDDCs, and 293FT-transfected cells were included as controls for flow cytometry, Western blot analysis, and the NF-κB reporter assay. HFFs and MDDCs were treated with 20 nM TNF-α (R&D Systems) 5 min prior to harvest. 293FT-transfected cells were treated with 20 nM TNF-α 24 h prior to analysis.

VZV infection of DCs. DCs were infected using VZV rOKA as previously described (2). Mock-infected DCs were prepared in parallel using uninfected HFFs as an inoculum.

Antibodies. Antibodies for human polyclonal NF-κB p50 and NF-κB p65 were obtained from Santa Cruz Biotechnology and used for immunofluorescence staining. Human IκBα, phosphorylated IκBα, NF-κB p50, and NF-κB p65 antibodies were obtained from Cell Signaling Technologies and used for Western blot analysis. Monoclonal α-tubulin used for Western blot analysis was obtained from Millipore and topoisomerase II (Ab-1) from Merck (Australia). Monoclonal TLR3-fluorescein isothiocyanate (FITC)-conjugated (clone 40C1285.6), TLR8-FITC (clone 44C143), and TLR9-FITC (clone 26C593.2) antibodies were obtained from Imgenex. Monoclonal CD1a-allophycocyanin (APC)-conjugated and CD14-FITC-conjugated antibodies were obtained from BD Biosciences (Australia). CD120a (TNF-Rec p55) (clone MR1-2) and CD120b (TNF-Rec p75) were obtained from Biodesign and Caltag, respectively. Anti-HA-Alexa Fluor 647 antibody was obtained from Cell Signaling Technologies. Antibodies used to detect VZV antigens were VZV glycoprotein E (gE; Chemicon, Australia), VZV gB (Biodesign), and VZV-mixed epitope-FITC (Biodesign). Isotype control antibodies included mouse monoclonal IgG1-APC (BD Biosciences), mouse monoclonal IgG2aκ-PE (Pharmingen), mouse monoclonal IgG2a-FITC (Caltag), and normal rabbit IgG (Santa Cruz Biotechnology).

Flow cytometry. MDDCs were washed twice in 1× phosphate-buffered saline (PBS) and fixed using 1% paraformaldehyde (PFA) for 15 min. The cells were washed twice in 1× PBS before permeabilization using 0.5% saponin (Sigma-Aldrich, Australia) in 1× PBS containing 1% FBS at 10^5 cells/100 μl for 15 min at room temperature. Primary antibodies were diluted 1:50 for anti-human TLR3-FITC, TLR8-FITC, and TLR9-FITC and 1:200 for VZV gB in 0.5% saponin-PBS. Secondary antibody for gB, goat anti-mouse-PE was diluted 1:200 in 0.5% saponin-PBS. Primary and secondary antibody incubations were for 20 min at room temperature in the dark. The cells were washed twice in 0.5% saponin-PBS between each incubation with a final resuspension in fluorescence-activated cell sorting (FACS) buffer (1× PBS containing 1% FBS and 0.2% sodium azide) before acquisition using FACScanto (Becton Dickinson) and analysis using FlowJo analysis software. The cells were incubated with the appropriate isotype control antibodies in parallel. A signal exceeding the level of 98% of the isotype control cell sample was considered to be positive for the cell-specific antibody staining.

TNF-α-stimulated 293FT cells cotransfected with hemagglutinin (HA)-tagged expression constructs and pNFκB-hrGFP reporter (Stratagene/Agilent Technologies, Australia) were washed twice in 1× PBS and fixed using 1× PBS containing 1% PFA. Cells were washed twice in 1× PBS before permeabilization using 100% ice-cold methanol incubated at −20°C for 30 min. Cells were washed twice in 1× PBS and resuspended in FACS buffer. Anti-HA-Alexa Fluor 647 antibody was diluted 1:50 in FACS buffer and incubated for 30 min at room temperature. The cells were washed twice in FACS buffer and resuspended in 400 μl of FACS buffer prior to analysis with FACScanto and FlowJo software. 293FT cells not exposed to TNF-α and no-plasmid DNA transfection controls were performed in parallel.

FACS. Cells were washed twice in 1× PBS and resuspended in 500 μl of FACS buffer per 2.5×10^6 cells. Anti-CD1a-APC (20 μl/2.5×10^6 cells) and anti-VZV-mixed epitope-FITC (3.5 μl/2.5×10^6 cells) primary antibodies were incubated for 20 min at 4°C in the dark. The cells were washed three times in FACS buffer, resuspended in FACS buffer (3×10^6 cells/ml), and sorted immediately using FACS Vantage (Becton Dickinson). Cells were sorted to positively select for $CD1a^+$ VZV^+ cells. To establish nonspecific background staining, the cells were incubated with appropriate isotype control antibodies, and a signal exceeding the level of 98% of the isotype control cell sample was considered to be positive for the cell surface-specific antibody staining. Mock-infected cells were stained in parallel using CD1a-APC antibody only and sorted for $CD1a^+$ cells. The purity of DCs after sorting was typically >98% for mock-infected DCs and >93% for VZV-infected DCs. Sorted DCs were used for subsequent immunofluorescence staining or Western blot analyses.

Western blot. Cells were incubated for 10 min in lysis buffer (50 mM Tris [pH 7.4], 240 mM NaCl, 0.5% NP-40, 10% glycerol, and 0.1 mM EDTA) containing a protease inhibitor cocktail (Roche, Australia). Cell lysates for immunoblotting with phospho-specific antibodies were lysed using PhosphoSafe extraction reagent (Merck, Australia) according to the manufacturer's instructions. Proteins were resolved by 12% polyacrylamide gels (Bio-Rad, Australia), transferred to Hybond-P polyvinylidene difluoride (PVDF) membrane (Amersham, United Kingdom), with nonspecific sites blocked using 5% skim milk powder in 1× TBST (Tris-buffered saline containing 0.1% Tween 20) for at least 1 h. Primary antibodies were incubated for 1 h or overnight diluted in 5% skim milk powder or 5% bovine serum albumin-TBST, respectively. Membranes were washed in 1× TBST for three 5-min intervals, and secondary antibody conjugated to horseradish peroxidase was incubated for 1 h, followed by three 5-min TBST washes, and exposed using the ECL Plus detection system (GE Healthcare, Australia). Densitometry was performed using Kodak Image Station 4000MM (Carestream Health, Inc.) to quantify the relative protein amounts detected by Western blotting.

Immunofluorescence staining and confocal microscopy. Immunofluorescence staining was performed as previously described (15). At least 2×10^5 cells were spotted onto glass slides. Primary antibodies were incubated for 1 h at room temperature, and secondary antibodies were incubated for 45 min. Slides were mounted using Prolong Slowfade Gold with DAPI (4′,6′-diamidino-2-phenylindole; Invitrogen), and confocal analysis was performed using an Olympus FV1000 confocal microscope. The percentages of cells with NF-κB p50 or p65 nuclear localized staining were determined by counting 100 cells per slide.

Plasmids and transfection. A series of plasmids was used, developed in the vector pGK2-HA (parental construct) (11), and designated pGK2-ORF61-HA, pGK2-ORF64-HA, pGK2-ORF47-HA, pGK2-ORF2-HA, pGK2-ORF21-HA, pGK2-ORF23-HA, and pGK2-ORF49-HA depending

on the indicated ORF. Each was generated by PCR amplification of the complete ORF from VZV, using primers designed with flanking restriction sites (either EcoRI or MfeI at the amino end and either BclI, BamHI, or BglII at the 3′ end) for ligation into the pGK2-HA construct. All ORFs contain an amino-terminal HA tag for antibody recognition. Plasmid pIRES2-ORF61-DsRED2 was generated by PCR amplification of the complete ORF61 sequence from VZV S strain, using primers designed with flanking EcoRI and BamHI sites to facilitate cloning into EcoRI and BamHI sites of pIRES2-DsRED2 (Clontech). Fugene HD (Promega) was utilized for transfection of 293FT cells according to the manufacturer's instructions using a DNA/Fugene ratio of 2:6. The cells were seeded 24 h prior to transfection, so they were 30% confluent at time of transfection. Transfected cells were harvested at 48 h posttransfection and analyzed by flow cytometry or Western blot analysis.

Site-directed mutagenesis. QuikChange II XL site-directed mutagenesis kit (Stratagene/Agilent Technologies) was used to construct pIRES2-ORF61 C19G (C19G; disrupt RING finger) (31), pIRES2-ORF61 Q62_START (M1T, M23T, M33T, and Q62M; express following RING finger domain), pIRES2-ORF61 Q62_STOP (Q62Stop; express RING finger domain), and pIRES2-ORF61 Q139_STOP (Q139Stop; express E3 ubiquitin ligase domain) according to the manufacturer's instructions. Primers were designed using PrimerX software, with sequences available upon request. All mutations were confirmed by sequencing using Australian Genome Research Facility. Protein expression was confirmed by flow cytometry and Western blot analysis.

NF-κB reporter assay. The day prior to transfection 293FT cells were seeded into six-well plates so they were 30% confluent at time of transfection. The cells were transfected using Fugene HD with 2 μg of pNFκB-hrGFP (Stratagene/Agilent Technologies) reporter construct and 1 μg of DsRED2- or HA-tagged expression construct. TNF-α (20 nM) was added at 24 h posttransfection, followed by additional culture for a further 24 h before the cells were harvested and analyzed by flow cytometry using FACScanto and FlowJo software as described above. The percentages of VZV ORF$^+$ GFP$^+$ cells were normalized to the respective parental plasmid, pIRES2-DsRED2 or pGK2-HA.

RESULTS

VZV infection prevents NF-κB p50 and p65 translocation into the nuclei of DCs. VZV infection of immature DCs inhibits their maturation *in vitro* (2). It has also been reported that VZV actively inhibits NF-κB signal transcription pathways within infected fibroblasts *in vitro* and *in vivo* (17). Given the importance of NF-κB signal transduction pathways in regulating expression of functionally important immune molecules expressed by DCs, we sought to determine whether VZV modulated NF-κB signaling within human DCs.

We first investigated the cellular localization of the NF-κB subunits, p50 and p65, via immunofluorescent staining and confocal microscopy, within VZV-infected DCs. Human MDDCs were infected using an established cell-associated method of infection by using VZV rOKA-infected fibroblasts (HFFs) to infect immature DCs at a DC/fibroblast ratio of 2:1 (2, 22). DCs were differentiated from the HFF inoculum using CD1a immunostaining, a marker for DCs (2). Since our infection protocol does not result in 100% of the DCs becoming infected (2), the cells were also stained with anti-VZV antigen antibody (VZV-mixed epitope-FITC) and subjected to FACS to select for VZV$^+$ CD1a$^+$ DCs. The purity of VZV$^+$ CD1a$^+$ sorted populations was typically 93 to 98%. Mock-infected MDDCs were immunostained in parallel, and CD1a$^+$ cells were isolated by FACS. Figure 1 shows the localization of p50, and Fig. 2 shows the distribution of the p65 subunit.

VZV-infected DCs and mock-infected DCs were spotted onto glass microscope slides, fixed, permeabilized, and stained with anti-NF-κB p50 or p65 antibody (red), along with an anti-VZV gE antibody (green). In parallel, this staining was also performed on TNF-α-treated uninfected HFFs and uninfected DCs (as positive controls for activation of the NF-κB pathway), uninfected HFFs (as a negative control for activation of the NF-κB pathway), as well as VZV-infected HFFs, as a control for the inhibition of NF-κB activation (17). In parallel, duplicate cell spots were stained with isotype control antibodies to establish background fluorescence. All immunostained slides were then analyzed by confocal microscopy.

Mock-infected DCs did not stain for VZV antigens, and the majority of the cells showed predominant cytoplasmic localization of NF-κB p50 and p65 subunits, indicating an inactive NF-κB pathway (Fig. 1A and 2A). On average, 31 and 29% of the mock-infected DCs showed nuclear staining for NF-κB p50 and p65, respectively. NF-κB p50 and p65 localized to the nucleus in 100% of DCs treated with TNF-α (Fig. 1B and 2B), a finding consistent with activation of the NF-κB pathway. In stark contrast, VZV$^+$ CD1a$^+$ DCs showed an average of only 8% of cells with NF-κB p50 localized to the nucleus (Fig. 1C). NF-κB p65 within VZV$^+$ CD1a$^+$ DCs localized predominantly to the cytoplasm with no detectable nuclear location (Fig. 2C). This indicates that VZV prevents NF-κB subunits from translocating into the nucleus of VZV antigen-positive cells. In a side-by-side comparison, the NF-κB pathway within unstimulated HFFs was predominantly inactive, as demonstrated by cytoplasmic NF-κB p50 and NF-κB p65 staining within 67 and 100% of the uninfected cells, respectively (Fig. 1D and 2D), and active within TNF-α-treated HFFs, with NF-κB p50 localized to the nucleus of 83% of cells and NF-κB p65 localized to the nucleus of 100% of cells within this group (Fig. 1E and 2E). In VZV infection of HFFs, typically 80% of the HFFs were positive for VZV antigen, and an average of 20% of VZV antigen-positive HFFs showed NF-κB p50 localized to the nucleus, with 4% of cells with nuclear localized NF-κB p65 (Fig. 1F and 2F), suggesting that the NF-κB pathway is predominantly inactive within these cells. We conclude that VZV efficiently prevents nuclear localization of NF-κB subunits in DCs.

Four replicate experiments were quantified for the percentages of cells with nuclear localization of NF-κB proteins (Fig. 1G and 2G). The VZV-infected DCs had a greatly reduced ability to activate the NF-κB pathway, as indicated by the predominant cytoplasmic localization of both NF-κB p50 and p65 subunits. Taken together, these results establish VZV modulation of the NF-κB pathway by sequestering NF-κB protein subunits, p50 and p65 in the cytoplasm of infected DCs.

VZV does not downmodulate the expression of NF-κB pathway stimulatory receptors—TLR3, TLR8, TLR9, TNFR-1 or TNFR-2—within infected DCs. The NF-κB pathway was subsequently examined for upstream events known to trigger NF-κB p50 and p65 nuclear translocation. Immune receptors that stimulate the NF-κB pathway include Toll-like receptors (TLRs) and tumor necrosis factor receptors (TNFRs) (26), so mock-infected or VZV-infected DCs at 48 h postinfection were costained for VZV antigen (VZV gB) and TLR3, TLR8, TLR9, TNFR-1, or TNFR-2 in conjunction with the DC cell surface marker CD1a. We have previously demonstrated that VZV infection of DCs does not affect the cell surface expression of this molecule on DCs (2). Additional controls consisted of mock-infected and VZV-infected DCs immunostained with isotype control antibodies. The cells were then analyzed by flow cytometry to determine the level of

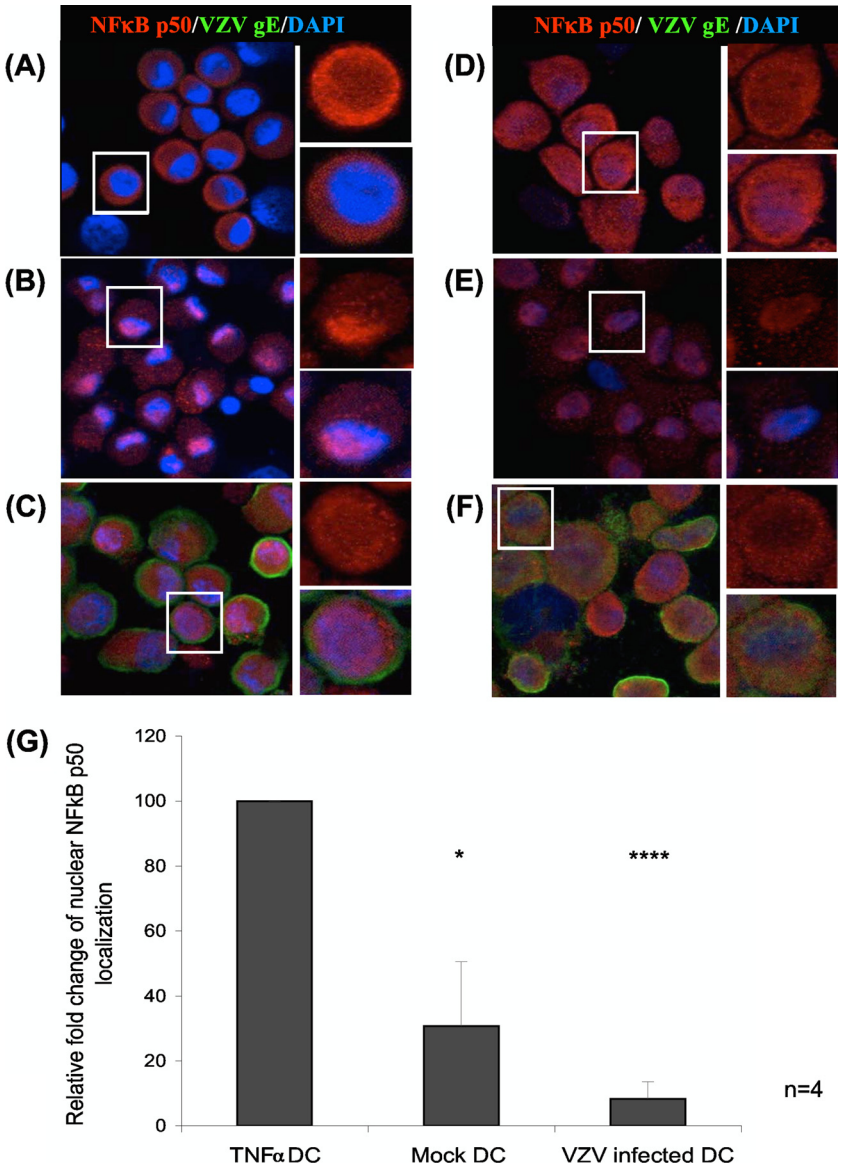

FIG 1 Cellular localization of NF-κB p50 determined by immunofluorescent staining and confocal microscopy. NF-κB p50 subunit cellular localization was determined within DCs (A to C) and HFFs (D to F) that were either mock infected (A and D), TNF-α (20 nM 5 min) stimulated (B and E), or VZV infected (C and F). Cells were harvested at 48 h postinfection. DCs were fluorescence activated cell sorted for $CD1a^+$ cells within the mock-infected population or VZV^+ $CD1a^+$ cells from the infected population. Sorted cells were stained with an antibody against NF-κB p50 (red), VZV gE (green), and DAPI nuclei (blue). Three-color images are shown on the left, with magnified inserts of NF-κB p50 alone in the upper right portion of the figure and three-color magnified inserts in the lower right portion. Nuclear localization of NF-κB p50 is indicative of an active NF-κB pathway. The percentages of cells with NF-κB p50 localized to the nucleus were determined by analysis of 100 cells per slide (G). Statistical significance was determined by using the Student *t* test (*, $P < 0.05$; ****, $P < 0.00005$).

expression of each cellular marker on VZV antigen-positive DCs. The mean fluorescence intensities of immune molecule expression by VZV antigen-positive DCs from three independent replicate experiments were averaged and normalized to mock-infected DCs (Fig. 3). There was no significant difference in the levels of expression of TLR3, TLR8, TLR9, TNFR-1, or TNFR-2 when we compared VZV-infected DCs to mock-infected DCs. These results demonstrate that VZV infection does not inhibit the expression of the NF-κB signaling receptors TLR3, TLR8, TLR9, TNFR-1, or TNFR-2 by DCs, suggesting the NF-κB pathway may be modulated downstream of these signaling receptors.

VZV infection of DCs induces phosphorylation of IκBα. The activation of the NF-κB pathway routinely involves phosphorylation of IκB, leading to its ubiquitination and degradation (14, 26). To assess IκB phosphorylation, DCs were mock infected or VZV infected and, at 48 h postinfection, were first immunostained for VZV antigen and CD1a. VZV^+ $CD1a^+$ DCs from infected DC cultures and $CD1a^+$ DCs from mock-infected cultures were separated from any remaining HFF inoculum by FACS and then lysed, and the protein extracts were examined by SDS-PAGE and Western blot with antibodies against IκBα or phosphorylated IκBα (Fig. 4, phos IκBα). The relative amounts of each protein were determined by densitometry with all values normalized to expression of α-tubulin, which was included as a protein loading

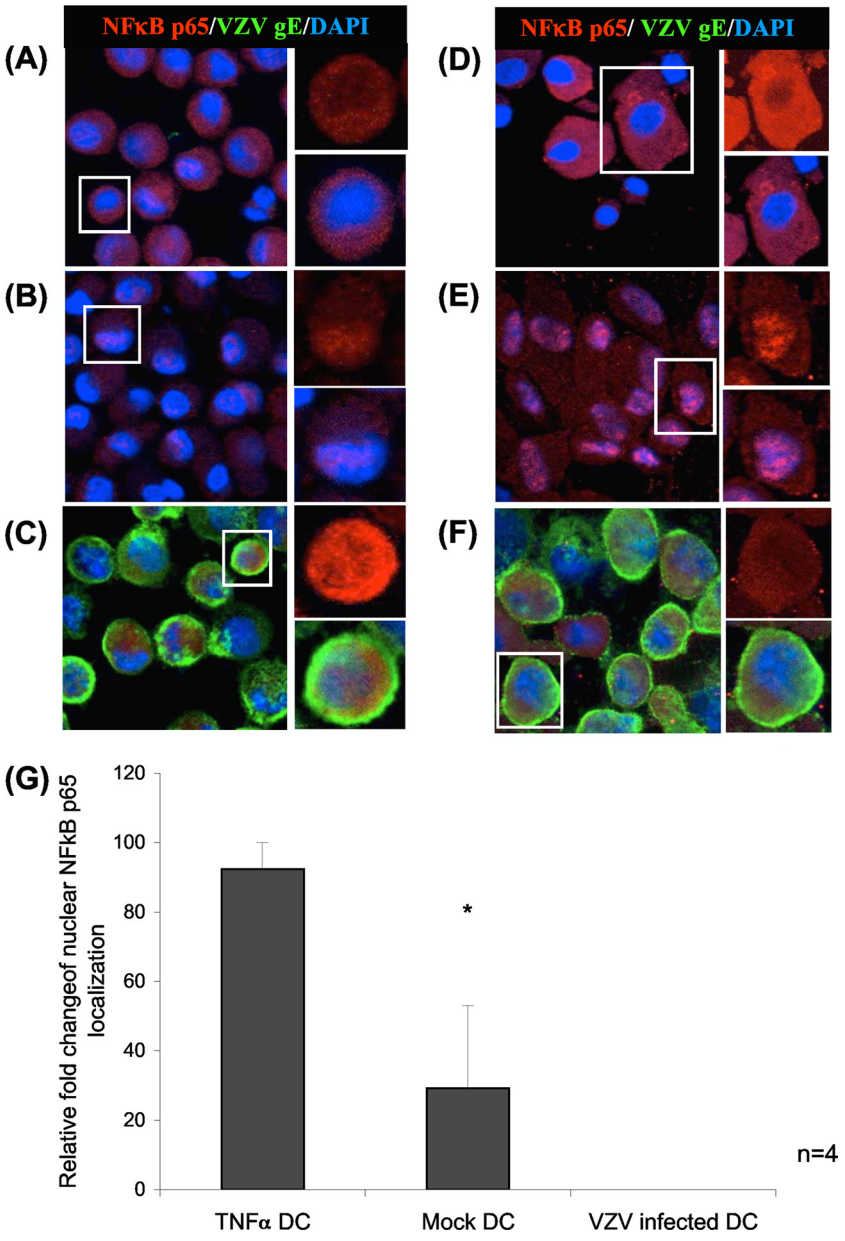

FIG 2 Cellular localization of NF-κB p65 protein subunits determined by immunofluorescence staining and confocal microscopy, as detailed in the legend to Fig. 1. Cellular localization of NF-κB p65 in DCs (A to C) and HFFs (D to F), either mock infected (A and D), TNF-α treated (20 nM, 5 min) (B and E), or VZV infected (C and F). NF-κB p65 (red), VZV gE (green), and DAPI nuclei (blue) are shown. (G) The percentages of cells with NF-κB p65 localized to the nucleus were determined by analysis of 100 cells per slide. The statistical significance was determined by using the Student *t* test (*, $P < 0.05$).

control (Fig. 4). In seven independent replicate experiments, it was observed that whereas unstimulated HFFs showed basal levels of phosphorylation and mock CD1a$^+$ DCs demonstrated the presence of low levels of phosphorylated IκBα (Fig. 4A), VZV$^+$ CD1a$^+$ DCs showed the presence of high levels of phosphorylated IκBα (Fig. 4A). The average densitometry measurements of seven replicate experiments, normalized to α-tubulin and then to mock-infected DC levels (Fig. 4B), showed that VZV$^+$ CD1a$^+$ DCs demonstrated a statistically significant increase in the expression of both IκBα and phosphorylated IκBα ($P < 0.05$). These data demonstrate that impairment of the NF-κB pathway in VZV-infected DCs is not a consequence of inhibited phosphorylation of IκBα since the pathway remains active at this step.

VZV ORF61 inhibits TNF-α induced NF-κB pathway activation. The inhibition of the NF-κB pathway in VZV-infected cells argues in favor of a viral gene product that encodes this function. To identify viral gene products that modulate the NF-κB pathway, we used a transient-transfection approach to assess the ability of individual VZV gene products to inhibit NF-κB activity. Due to the low transfection efficiency of DCs (30), 293FT cells were cotransfected with pNFκB-hrGFP reporter, along with a plasmid expressing, from the complete cytomegalovirus immediate-early promoter, one of several HA-tagged VZV ORFs: ORF2, ORF21, ORF23, ORF47, ORF49, ORF61, or ORF64. After 24 h, cotransfected cells were stimulated with TNF-α to activate the NF-κB pathway 24 h prior to harvest. The cells were also stained with

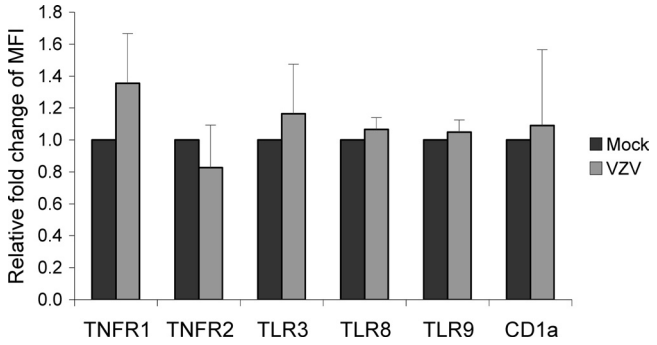

FIG 3 Mean fluorescence intensity (MFI) of the pattern recognition receptors TLR3, TLR8, or TLR9 or of surface TNFR-1 or -2 on VZV-infected DCs. VZV-infected DCs were harvested at 48 h postinfection and dual stained for intracellular TLR3, TLR8, or TLR9 or surface stained for TNFR-1 or -2, along with VZV gB. The MFI values were normalized to the respective mock-infected DCs. CD1a was included as a control since its expression should remain unchanged following infection.

anti-HA antibody prior to analysis by flow cytometry. The parental pGK2-HA construct without any VZV ORF expressed a level of green fluorescent protein (GFP) expression indicative of NF-κB pathway activation that was set as a value of 1. Three replicate experiments were averaged and normalized to values from the cells transfected with the pGK2-HA control and treated with TNF-α (Fig. 5). Relative to the control, plasmids expressing VZV ORFs (ORF64, ORF47, ORF2, ORF49, ORF21, and ORF23) did not significantly alter TNF-α-stimulated NF-κB reporter activity compared to the parental control. However, pGK2-HA VZV ORF61 showed a striking reduction in TNF-α-stimulated NF-κB reporter activity, with statistical significance ($P < 0.00005$). This suggested this viral gene product is at least in part, responsible for inhibiting the NF-κB pathway.

VZV ORF61 inhibits TNF-α-induced IκBα degradation. Phosphorylation of IκBα stimulates its ubiquitin-induced degradation, allowing NF-κB subunits to translocate into the nucleus

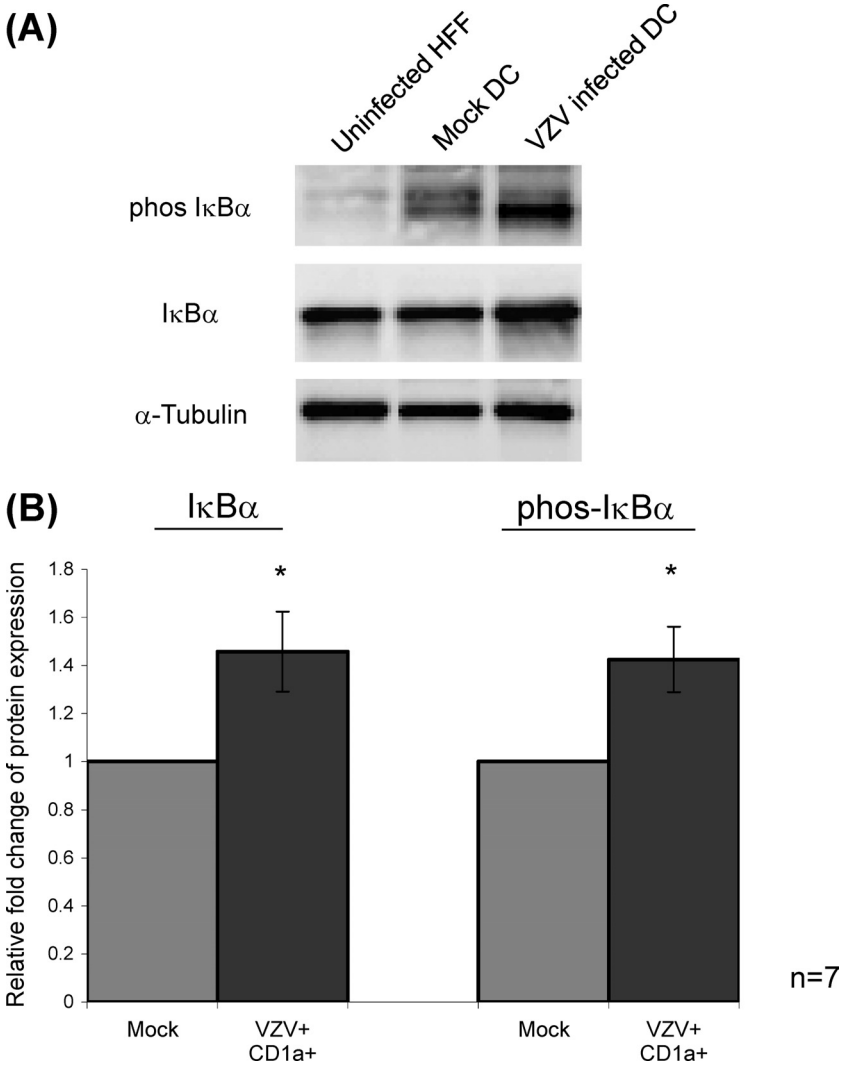

FIG 4 Analysis of IκBα phosphorylation following VZV infection of DCs. (A) Western blot analysis was performed on total cell lysates obtained from uninfected HFFs, mock-infected CD1a$^+$ DCs, and VZV antigen-positive CD1a$^+$ DCs separated on a 12% polyacrylamide gel and transferred to PVDF membrane. Blots were probed with antibodies specific for IκBα or phosphorylated IκBα. All blots were also probed with an antibody against α-tubulin as a protein loading control. (B) The results from seven independent replicate experiments were averaged and normalized to α-tubulin by densitometry, and the statistical significance was determined using the Student *t* test (*, $P < 0.05$).

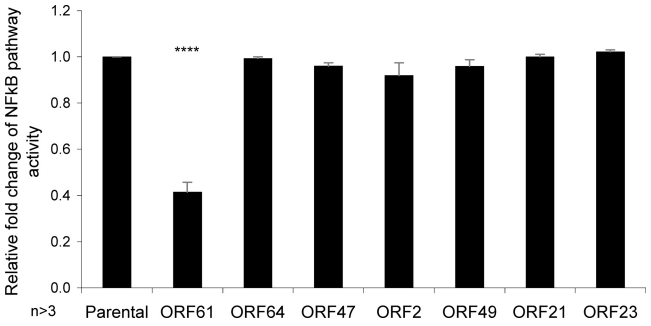

FIG 5 Identification of a viral gene product responsible for inhibiting TNF-α-stimulated NF-κB pathway activation. 293FT cells were cotransfected with pNFκB-hrGFP reporter construct and either pGK2-HA-ORF61, -ORF64, -ORF47, -ORF2, -ORF49, -ORF21, or -ORF23. The cells were stimulated with TNF-α (20 nM) at 24 h posttransfection and analyzed by flow cytometry at 48 h posttransfection. The level of GFP expression within HA expressing cells was then determined using GFP expression representing NF-κB pathway activity. Replicate experiments were averaged and normalized to the parental control, pGK2-HA, with statistical significance obtained using the Student *t* test (****, $P < 0.00005$).

for transcription of target genes (5). However, no decrease in IκBα was seen following VZV infection of DCs, and the phosphorylation of IκBα was readily detected. With the identification of ORF61 as an inhibitor of NF-κB pathway activity, we sought to determine whether ORF61 functions to inhibit IκBα degradation, preventing subsequent NF-κB p50 and p65 translocation into the nucleus. 293FT cells transiently transfected with pGK2-ORF61-HA and cultured for 48 h, followed by TNF-α (20 nM, 5 min) stimulation, showed that IκBα protein was detected within all transfected 293FT cells following TNF-α stimulation (Fig. 6A). However, densitometric quantification of three replicate experiments, normalized to α-tubulin and then to levels in cells transfected with the parent construct (Fig. 6B), revealed that ORF61 expression construct (pGK2-ORF61-HA) had significantly more IκBα protein present following TNF-α stimulation compared to the parental construct control ($P < 0.05$). These findings indicate either that ORF61 protects IκBα protein from TNF-α-induced degradation, further defining the mechanism of ORF61-mediated NF-κB pathway inhibition, or that ORF61 upregulates the expression of IκBα, which is consistent with previous cell-specific transcriptional activation.

The E3 ubiquitin ligase domain of ORF61 is responsible for inhibiting TNF-α-induced NF-κB pathway activation. To explore the ORF61 inhibition of TNF-α-stimulated NF-κB reporter activity further, ORF61 was expressed using a vector, pIRES2-DsRED2, in which DsRED2 is a second reporter of activity of expression. In the NF-κB reporter assay, TNF-α-stimulated pIRES2-DsRED2-ORF61 expressing 293FT cells re-

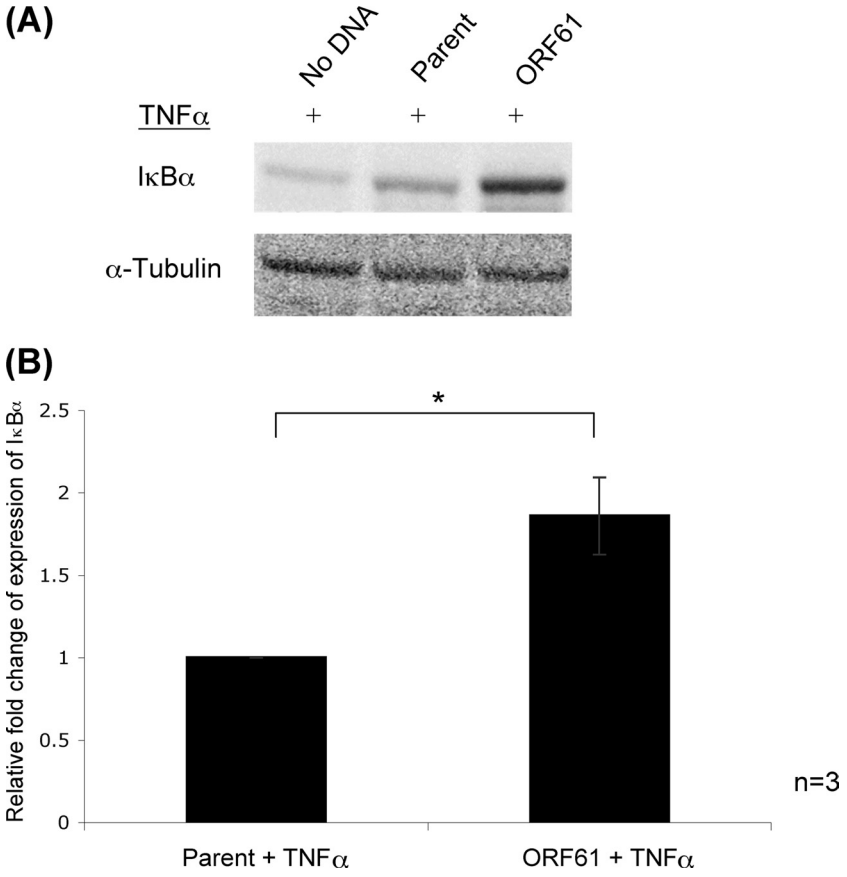

FIG 6 Impact of ORF61 on TNF-α-induced levels of IκBα protein. (A) Western blot analysis performed on total cell lysates from 293FT cells transfected with pGK2-ORF61-HA cells and stimulated with TNF-α 48 h posttransfection. The proteins were separated by SDS-PAGE, membranes were probed with an antibody against IκBα. pGK2-HA (parent construct), and no DNA transfected cells were included as controls. (B) Densitometry was performed to determine the relative levels of protein expression, with results averaged and normalized to α-tubulin, which was included as a protein loading control. The results are presented relative to the parental control. Statistical significance was determined using the Student *t* test (*, $P < 0.05$).

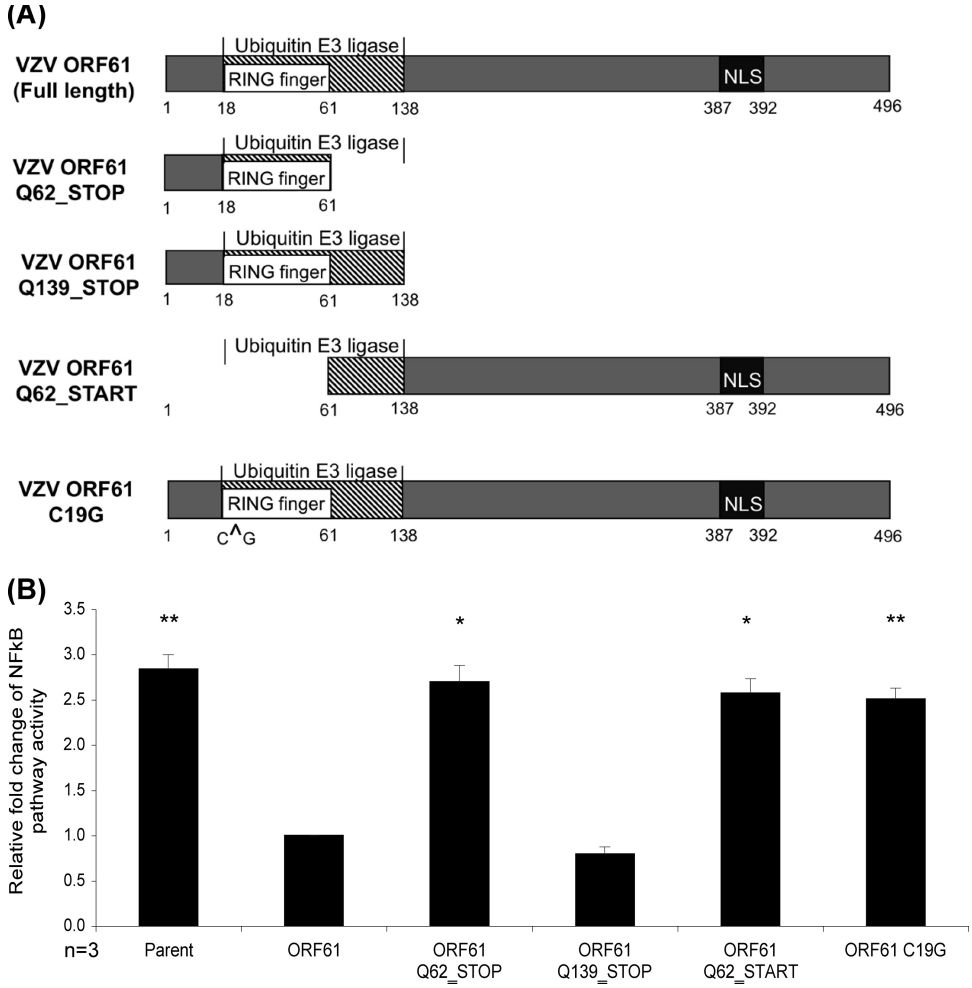

FIG 7 Mutation of ORF61 to identify domains mediating NF-κB inhibition. (A) Depiction of ORF61 mutants generated using site-directed mutagenesis of pIRES2-DsRED2-ORF61 constructs. ORF61-DsRED2 full-length shows the functionally important regions of ORF61. ORF61 Q62_STOP truncates ORF61 following its RING finger domain. ORF61 Q139_STOP is truncated following the E3 ubiquitin ligase domain, ORF61 Q62_START is transcribed following the RING finger domain, and ORF61 C19G contains an amino acid substitution within its RING finger domain reported to disrupt its function. NLS, nuclear localization signal. (B) Mutant ORF61-DsRED2 expressing constructs were cotransfected along with pNFκB-hrGFP reporter construct into 293FT cells, stimulated with TNF-α (20 nM) at 24 h posttransfection, and cultured for a further 24 h before being analyzed by flow cytometry for GFP expression within DsRED2$^+$ cells. GFP expression is indicative of NF-κB pathway activity. Replicate experiments were averaged and normalized to full-length ORF61. Statistical significance was determined by using the Student *t* test (*, $P < 0.05$; **, $P < 0.005$).

producibly showed an average 65% reduction in NF-κB reporter activity compared to pIRES2-DsRED2 parental control, with statistical significance ($P < 0.005$) (Fig. 7B). Subsequent site-directed mutagenesis was performed to produce mutations within functionally important regions of ORF61 coding sequence within the pIRES2-DsRED2-ORF61 vector (Fig. 7A). These ORF61 mutant constructs were cotransfected along with pNFκB-hrGFP reporter into 293FT cells, stimulated with TNF-α 24 h posttransfection, and cultured for a further 24 h. Transfected cells were analyzed by flow cytometry, gating for GFP$^+$ DsRED2$^+$cells, with GFP expression indicative of an active NF-κB pathway. The results from three replicate experiments were averaged and normalized to cells cotransfected with the full-length ORF61 construct (Fig. 7B).

As shown for HA-tagged ORF61 expressing cells (Fig. 5), cells expressing the full-length ORF61 displayed significantly decreased NF-κB reporter activity compared to the parental control, pIRES2-DsRED2 ($P < 0.005$). In contrast, the ORF61 mutant constructs ORF61 Q62_STOP, ORF61 Q62_START, and ORF61 C19G lost their capacity to inhibit the TNF-α-stimulated NF-κB reporter activity. Only cells transfected with the ORF61 Q139_STOP construct, which encompasses the E3 ubiquitin ligase domain, retained the capacity to inhibit the NF-κB pathway to the level of inhibition seen for full-length ORF61. Based on the protein regions expressed, these results indicate the E3 ubiquitin ligase domain of ORF61 is required to mediate an inhibition of the NF-κB pathway. Of note is that a single point mutation in the ORF61 RING finger domain, known to disrupt the E3 ubiquitin-like activity (31), lost the capacity to inhibit the TNF-α-stimulated NF-κB reporter activity.

DISCUSSION

This study identifies VZV-encoded modulation of the NF-κB signaling pathway within infected DCs and identifies the viral gene product of ORF61 as functioning to inhibit this important signal

transduction pathway. Given that DCs are proposed as the first immune cells to encounter VZV following inoculation, these results indicate that ORF61 plays an important role in immune evasion of the NF-κB signal transduction pathway. This pathway controls transcription of many immune molecules required to initiate an immune response to foreign pathogens, and so disruption of this pathway is likely to suppress critical immune effector capacity of the host cell.

Other herpesviruses modulate the NF-κB pathway in a cell type-dependent manner (3, 9, 19, 23, 24, 27, 28, 34). Our work indicates VZV modulates the NF-κB pathway within DCs. The cytoplasmic retention of NF-κB protein subunits p50 and p65 indicates that the pathway is modulated prior to their translocation into the nucleus, as shown by immunofluorescence and confocal microscopy. These results are distinct from those reported for HSV-1 infection, where NF-κB proteins are translocated into the nucleus of HSV-1-infected C33-A cells (24). The NF-κB pathway in VZV-infected DCs was not modulated by downregulation of TLR3, TLR8, TLR9, TNFR-1, or TNFR-2, which signal the activation of the NF-κB pathway, since these were unaffected by VZV infection. This finding is consistent with VZV interfering with NF-κB signaling at a point downstream of cell surface (TNFR-1 and TNFR-2) or intracellular receptors which trigger this pathway (TLR3, TLR8, and TLR9).

A critical component of activation of the NF-κB pathway is phosphorylation of IκBα (5). We therefore explored the phosphorylation state of IκBα in infected DCs. The increase in phosphorylated IκBα within VZV-infected DCs indicated that the NF-κB pathway was able to be activated at this level following infection. In addition, IκBα protein levels within DCs did not decrease following infection with VZV. Thus, IκBα can be phosphorylated and is not necessarily degraded following VZV infection of DCs. The NF-κB pathway is therefore apparently inhibited following phosphorylation of IκBα but prior to translocation of NF-κB p50 and p65 into the nucleus of VZV-infected DCs. The identification of this step is under further consideration.

We identified VZV ORF61 as a gene responsible for inhibiting TNF-α-stimulated NF-κB reporter expression. VZV ORF61 is transcribed within 1 h of infection; however, it is not a component of the virion, supporting reports of UV-inactivated VZV being unable to inhibit the NF-κB pathway within fibroblasts and that *de novo* gene synthesis is required (17, 18, 33). ORF61 has also been implicated in the modulation of other cellular pathways, such as the mitogen-activated protein kinase (MAPK) pathways where a significant increase in the phosphorylation of JNK/SAPK and a decrease in p38/MAPK phosphorylation were observed in MeWo cells transfected with ORF61 (25). ORF61 also downmodulates the IRF3-mediated IFN-β pathway by its direct binding to and degradation of IRF3 (35). We demonstrate that when ORF61 is expressed alone, it is sufficient to inhibit TNF-α-induced IκBα degradation, further defining the role of ORF61 in NF-κB pathway inhibition. We also showed that the E3 ubiquitin ligase domain of ORF61 is essential for NF-κB pathway inhibition, since mutations within this domain rendered ORF61 unable to inhibit NF-κB reporter activity. HSV-1 ICP0 and VZV ORF61 share homology within their RING finger domains, which are involved in E3 ubiquitin ligase activity (21). ICP0 modulates the NF-κB pathway in a cell type-dependent manner, as shown by transfection of ICP0 expression constructs into SHSY-5Y and HEK293 cells. Within HEK293 cells stably expressing either TLR2 or TLR4, ICP0 causes inhibition of TLR-mediated NF-κB signaling (9). ICP0 inhibits the NF-κB pathway within these cells by binding and transporting the host cell protein USP7, a ubiquitin-specific protease, to the cytoplasm, where it deubiquitinates TRAF6 and IKKγ. The USP7 binding site on ICP0 is within the C-terminal region; due to the homology of ICP0 and ORF61 being restricted to the RING finger domain in the N terminus, it is unlikely that ORF61 encodes this USP7 binding region and therefore inhibits the NF-κB pathway in a manner different from that of its HSV-1 homologous protein in HEK293/TLR cells. Expression of ICP0 within SHSY-5Y cells stimulated NF-κB reporter activity through the E3 ubiquitin ligase action of ICP0, resulting in ubiquitination and subsequent degradation of IκBα (10). Our demonstration that the E3 ubiquitin ligase domain of ORF61 is responsible for the inhibition of NF-κB reporter activity indicates that it may be the process of ubiquitination causing the effect; however, protein expression analysis of IκBα within VZV-infected DCs suggests that IκBα is not degraded. The Vpu protein of HIV, however, blocks proteasome-dependent degradation of IκBα by binding to βTRCP in the E3 ubiquitin ligase complex that is involved in the regulated degradation of IκBα (7). This suggests that the E3 ubiquitin ligase activity of ORF61 may have an indirect effect on NF-κB proteins.

Although we have shown that ORF61 is a viral factor that downregulates NF-κB, we have not yet verified whether it is the only viral factor able to do this. This requires the construction of VZV that lacks the ORF61 protein, particularly in the amino-terminal ring finger domain. Such mutants have proven very difficult to develop. Using a VZV bacterial artificial chromosome (BAC) system, we found that VZV BAC constructs engineered to contain the amino acid substitution within the RING finger domain of ORF61 (C19G) or a stop codon inserted directly after the RING finger domain or a stop codon inserted directly following the E3 ubiquitin ligase domain all resulted in either failure to obtain any recombinant VZV or the reversion of the point mutation to the wild type (M. B. Yee and P. Kinchington, unpublished data). This mirrors previous reports of ORF61 playing an important role in virus replication (8, 33). Thus, although ORF61 has been identified as functioning to inhibit the NF-κB pathway, it remains possible that other VZV gene products may also encode a similar function. In addition, whether the E3 ubiquitin ligase activity of ORF61 exerts a direct effect on NF-κB proteins or whether it impacts on the cellular regulators of these transcription factors will be an important focus of future work to delineate the mode of action of ORF61 in suppressing NF-κB signaling. The continued presence of phosphorylated IκBα within VZV-infected DCs indicates that it is not being degraded. Therefore, it would be useful to also investigate ubiquitin/protease pathways that control the degradation of IκBα following NF-κB pathway activation.

In summary, we identify here inhibition of the NF-κB signal transduction pathway in VZV-infected human MDDCs, which occurs following phosphorylation of IκBα, but prior to the translocation of NF-κB p50 and p65 into the nucleus. We also demonstrate that the immediate-early gene ORF61 inhibits TNF-α-stimulated NF-κB reporter expression, indicating that this viral gene can inhibit NF-κB pathway activation. Furthermore, we show that the region of ORF61 important for its inhibitory affects on TNF-α-stimulated NF-κB reporter activity is the E3 ubiquitin ligase domain, indicating that it is the process of ubiquitination that causes this pathway inhibition. During the preparation of this

manuscript, Wang et al. (32) presented findings that ORF61 binds SUMO-1 via three SUMO-interacting motifs (SIMs) and that these SIMs were required for ORF61 binding to and disrupting of PML nuclear bodies (32). That study also reported that ORF61 can act as an inhibitor of TNF-α-induced NF-κB reporter activity in a transient-transfection assay within a melanoma cell line, supporting the results presented here. VZV-encoded modulation of the NF-κB pathway may be the mechanistic basis for the observed downregulation of immune molecules in VZV-infected DCs, an important immune evasion strategy of VZV.

ACKNOWLEDGMENTS

This study was supported by an Australian National Health and Medical Research (NHMRC) project grant awarded to A.A. and B.S. E.S. was the recipient of an Australian Postgraduate Award and Westmead Millennium Foundation Stipend Enhancement Award. P.K. was supported by National Institutes of Health grants EY08098 and NS064022, by unrestricted funds from the Eye and Ear Institute of Pittsburgh, and by Research to Prevent Blindness, Inc.

REFERENCES

1. **Abendroth A, Kinchington PR, Slobedman B.** 2010. Varicella-zoster virus immune evasion strategies. Curr. Top. Microbiol. Immunol. **342**: 155–171.
2. **Abendroth A, Morrow G, Cunningham AL, Slobedman B.** 2001. Varicella-zoster virus infection of human dendritic cells and transmission to T cells: implications for virus dissemination in the host. J. Virol. **75**: 6183–6192.
3. **Amici C, et al.** 2006. Herpes simplex virus disrupts NF-κB regulation by blocking its recruitment on the IκBα promoter and directing the factor on viral genes. J. Biol. Chem. **281**:7110–7117.
4. **Baldwin AS, Jr.** 1996. The NF-κB and I κB proteins: new discoveries and insights. Annu. Rev. Immunol. **14**:649–683.
5. **Beg AA, Baldwin AS, Jr.** 1993. The I κB proteins: multifunctional regulators of Rel/NF-κB transcription factors. Genes Dev. **7**:2064–2070.
6. **Blackwell TS, Christman JW.** 1997. The role of nuclear factor-κB in cytokine gene regulation. Am. J. Respir. Cell Mol. Biol. **17**:3–9.
7. **Bour S, Perrin C, Akari H, Strebel K.** 2001. The human immunodeficiency virus type 1 Vpu protein inhibits NF-κB activation by interfering with beta TrCP-mediated degradation of IκB. J. Biol. Chem. **276**: 15920–15928.
8. **Cohen JI, Nguyen H.** 1998. Varicella-zoster virus ORF61 deletion mutants replicate in cell culture, but a mutant with stop codons in ORF61 reverts to wild-type virus. Virology **246**:306–316.
9. **Daubeuf S, et al.** 2009. HSV ICP0 recruits USP7 to modulate TLR-mediated innate response. Blood **113**:3264–3275.
10. **Diao L, et al.** 2005. Herpesvirus proteins ICP0 and BICP0 can activate NF-κB by catalyzing IκBα ubiquitination. Cell. Signal. **17**:217–229.
11. **Eisfeld AJ, Yee MB, Erazo A, Abendroth A, Kinchington PR.** 2007. Downregulation of class I major histocompatibility complex surface expression by varicella-zoster virus involves open reading frame 66 protein kinase-dependent and -independent mechanisms. J. Virol. **81**:9034–9049.
12. **Foo SY, Nolan GP.** 1999. NF-κB to the rescue: RELs, apoptosis and cellular transformation. Trends Genet. **15**:229–235.
13. **Ghosh S, Karin M.** 2002. Missing pieces in the NF-κB puzzle. Cell **109**(Suppl):S81–S96.
14. **Ghosh S, May MJ, Kopp EB.** 1998. NF-κB and Rel proteins: evolutionarily conserved mediators of immune responses. Annu. Rev. Immunol. **16**:225–260.
15. **Hood C, Cunningham AL, Slobedman B, Boadle RA, Abendroth A.** 2003. Varicella-zoster virus-infected human sensory neurons are resistant to apoptosis, yet human foreskin fibroblasts are susceptible: evidence for a cell-type-specific apoptotic response. J. Virol. **77**:12852–12864.
16. **Huch JH, et al.** 2010. Impact of varicella-zoster virus on dendritic cell subsets in human skin during natural infection. J. Virol. **84**:4060–4072.
17. **Jones JO, Arvin AM.** 2006. Inhibition of the NF-κB pathway by varicella-zoster virus in vitro and in human epidermal cells in vivo. J. Virol. **80**: 5113–5124.
18. **Kinchington PR, Vergnes JP, Turse SE.** 1995. Transcriptional mapping of varicella-zoster virus regulatory proteins. Neurology **45**:S33–S35.
19. **Laherty CD, Hu HM, Opipari AW, Wang F, Dixit VM.** 1992. The Epstein-Barr virus LMP1 gene product induces A20 zinc finger protein expression by activating nuclear factor κB. J. Biol. Chem. **267**: 24157–24160.
20. **Miranda-Saksena M, Armati P, Boadle RA, Holland DJ, Cunningham AL.** 2000. Anterograde transport of herpes simplex virus type 1 in cultured, dissociated human and rat dorsal root ganglion neurons. J. Virol. **74**:1827–1839.
21. **Moriuchi H, Moriuchi M, Smith HA, Straus SE, Cohen JI.** 1992. Varicella-zoster virus open reading frame 61 protein is functionally homologous to herpes simplex virus type 1 ICP0. J. Virol. **66**:7303–7308.
22. **Morrow G, Slobedman B, Cunningham AL, Abendroth A.** 2003. Varicella-zoster virus productively infects mature dendritic cells and alters their immune function. J. Virol. **77**:4950–4959.
23. **Moutaftsi M, Brennan P, Spector SA, Tabi Z.** 2004. Impaired lymphoid chemokine-mediated migration due to a block on the chemokine receptor switch in human cytomegalovirus-infected dendritic cells. J. Virol. **78**: 3046–3054.
24. **Patel A, et al.** 1998. Herpes simplex type 1 induction of persistent NF-κB nuclear translocation increases the efficiency of virus replication. Virology **247**:212–222.
25. **Rahaus M, Desloges N, Wolff MH.** 2005. ORF61 protein of varicella-zoster virus influences JNK/SAPK and p38/MAPK phosphorylation. J. Med. Virol. **76**:424–433.
26. **Rahman MM, McFadden G.** 2011. Modulation of NF-κB signalling by microbial pathogens. Nat. Rev. Microbiol. **9**:291–306.
27. **Stewart S, et al.** 2004. Epstein-Barr virus-encoded LMP2A regulates viral and cellular gene expression by modulation of the NF-κB transcription factor pathway. Proc. Natl. Acad. Sci. U. S. A. **101**:15730–15735.
28. **Sylla BS, et al.** 1998. Epstein-Barr virus-transforming protein latent infection membrane protein 1 activates transcription factor NF-κB through a pathway that includes the NF-κB-inducing kinase and the IκB kinases IKKα and IKKβ. Proc. Natl. Acad. Sci. U. S. A. **95**:10106–10111.
29. **Vallabhapurapu S, Karin M.** 2009. Regulation and function of NF-κB transcription factors in the immune system. Annu. Rev. Immunol. **27**: 693–733.
30. **Van Tendeloo VF, et al.** 2001. Highly efficient gene delivery by mRNA electroporation in human hematopoietic cells: superiority to lipofection and passive pulsing of mRNA and to electroporation of plasmid cDNA for tumor antigen loading of dendritic cells. Blood **98**:49–56.
31. **Walters MS, Kyratsous CA, Silverstein SJ.** 2010. The RING finger domain of varicella-zoster virus ORF61p has E3 ubiquitin ligase activity that is essential for efficient auto-ubiquitination and dispersion of Sp100 containing nuclear bodies. J. Virol. **84**:6861–6865.
32. **Wang L, et al.** 2011. Disruption of PML nuclear bodies is mediated by ORF61 SUMO-interacting motifs and required for varicella-zoster virus pathogenesis in skin. PLoS Pathog. **7**:e1002157.
33. **Wang L, Sommer M, Rajamani J, Arvin AM.** 2009. Regulation of the ORF61 promoter and ORF61 functions in varicella-zoster virus replication and pathogenesis. J. Virol. **83**:7560–7572.
34. **Yurochko AD, Kowalik TF, Huong SM, Huang ES.** 1995. Human cytomegalovirus upregulates NF-κB activity by transactivating the NF-κB p105/p50 and p65 promoters. J. Virol. **69**:5391–5400.
35. **Zhu H, et al.** 2011. Varicella-zoster virus immediate early protein ORF61 abrogates IRF3-mediated innate immune response through degradation of activated IRF3. J. Virol. **85**:11079–11089.